pH-regulated Slo3 K^+ Channels: Properties of Unitary Currents

Xue Zhang, Xuhui Zeng, Xiao-Ming Xia, and Christopher J. Lingle

Department of Anesthesiology and Department of Anatomy and Neurobiology, Washington University School of Medicine, St. Louis, MO 63110

Here we have examined the voltage and pH dependence of unitary Slo3 channels and used analysis of current variance to define Slo3 unitary current properties over a broader range of voltages. Despite complexity in Slo3 channel openings that precludes simple definition of the unitary conductance, average current through single Slo3 channels varies linearly with voltage at positive activation potentials. Furthermore, the average Slo3 unitary current at a given activation potential does not change with pH. Consistent with macroscopic conductance estimates, the apparent open probability of Slo3 channel exhibits a pH-dependent maximum, with limiting values around 0.3 at the most elevated pH and voltage. Estimates of Slo3 conductance at negative potentials support a weaker intrinsic voltage dependence of gating than is observed for Slo1. For the pH-regulated Slo3 K^+ channel, the dependence of macroscopic conductance on pH suggests that the pH-sensitive mechanism regulates gating in an allosteric manner qualitatively similar to regulation of Slo1 by Ca^{2+}. Together, the results support the view that the regulation of macroscopic Slo3 currents by pH reflects regulation of gating equilibria, and not a direct effect of pH on ion permeation. Specifically, both voltage and pH regulate a closed–open conformational change in a largely independent fashion.

The Journal of General Physiology

INTRODUCTION

A common characteristic of the various K^+ channels encoded by genes within the Slo family (Adelman et al., 1992; Butler et al., 1993) is their regulation by distinct cytosolic ligands: Ca^{2+} for Slo1 (Adelman et al., 1992; Butler et al., 1993), pH for Slo3 (Schreiber et al., 1998), and Na^+ for Slo2.1 and Slo2.2 (Bhattacharjee et al., 2002, 2003; Yuan et al., 2003). Although Slo family channels contain a pore domain with homology to voltage-dependent K^+ channels (Adelman et al., 1992; Butler et al., 1993), each subunit also contains an extensive C-terminal structure (Jiang et al., 2002) that is thought to be the main determinant for regulation by cytosolic ligands (Wei et al., 1994; Schreiber and Salkoff, 1997; Shi et al., 2002; Xia et al., 2002, 2004). For the most well-studied member of this channel family, Slo1, extensive investigations of the voltage and Ca^{2+} dependence of the so-called BK (large conductance Ca^{2+}-activated K^+) currents have suggested that voltage and Ca^{2+} have largely independent allosteric effects on the closed–open (C-O) conformational change (Horrigan and Aldrich, 2002). The pH dependence of Slo3 also arises from its cytosolic domain (Xia et al., 2004). However, the mechanisms by which changes in pH are coupled to regulation of Slo3 function remain unknown.

In the associated paper (see Zhang et al. on p. 317 of this issue), we examined the dependence of Slo3 macroscopic current on voltage and pH. Mechanistic evaluation of the pH and voltage dependence of the macroscopic currents depends on the assumption that pH and voltage only influence channel open probability (P_o) and not single channel conductance (g) or numbers of channels (N). Previous work indicated that Slo3 has a unitary conductance of ~90 pS (Wei et al., 1994; Schreiber and Salkoff, 1997; Shi et al., 2002; Xia et al., 2002, 2004), but difficulties in recording Slo3 channel activity precluded an extensive examination of Slo3 properties. Therefore, here we ask, does the Slo3 single channel current behave ohmically and is the unitary conductance independent of pH? The results support the view that the effects of pH on Slo3 involve the allosteric regulation of channel function and not effects on single channel conductance.

Correspondence to Christopher J. Lingle: clingle@morpheus.wustl.edu

MATERIALS AND METHODS

Oocyte Removal and Culture

The procedures for preparation and injection of stage IV *Xenopus laevis* oocytes follow standard methods in use in this lab (Xia et al., 2004). For single channel currents, mSlo3 RNA (at 1 μg/μl) was diluted 20-fold and oocytes were used at 1–3 d after injection.

Chimeric Constructs and Mutations

The mSlo3 construct (Schreiber et al., 1998) was provided by L. Salkoff (Washington University School of Medicine) and was modified as previously described (Xia et al., 2004). Sequencing of this construct resulted in a predicted protein sequence that differed from that previously published (Schreiber et al., 1998), but in agreement with sequence information based on the mouse genome project. The newer sequence replaces 57 residues at the C terminus with 66 residues. Updated information regarding the Slo3 cRNA and amino acid sequence can be accessed through accession no. AF039213 at http://www.ncbi.nlm.nih.gov/entrez/viewer.fcgi?val=AF039213.2.

Electrophysiological Methods

Standard excised inside-out patches were used for all experiments in this paper (Hamill et al., 1981). Currents were monitored using an Axopatch 200 amplifier (Molecular Devices) and voltage commands and data acquisition were accomplished with the Clampex program from the pClamp software package (Molecular Devices). Gigaohm seals were formed in normal frog Ringer (in mM, 115 NaCl, 2.5 KCl, 1.8 CaCl2, 10 HEPES, pH 7.4). Excised patches were moved into flowing test solutions to control the solution bathing the membrane face. The standard pipette/extracellular solution was (in mM) 140 K-methanesulfonate, 20 KOH, 10 HEPES, 2 $MgCl_2$, pH 7.0. The composition of solutions bathing the cytoplasmic face of the patch membrane contained (in mM) 140 K-methanesulfonate, 20 KOH, 10 HEPES, with the pH adjusted to the nominal values indicated in the text. In separate experiments, a triple buffer solution using HEPES, MES, and TABS was found to yield identical results to the solutions in which only HEPES was included. Procedures for solution application used a perfusion pipette with a 100–200-μ tip packed with seven PE10 tubes. Each tube was under separate valve control and solution flowed continuously from only one PE10 tube at a time onto the excised patch.

Data Analysis

Analysis of current recordings was accomplished either with Clampfit (Molecular Devices) or with programs written in this laboratory. For single channel recordings, currents were acquired at 100 kHz sampling rates and filtered at 10 kHz, unless otherwise indicated. Capacity currents were subtracted off-line either using a voltage step to 0 mV or adjacent null sweeps.

Analysis of Current Variance

For analysis of current variance, currents activated in sets of usually 100 identical activation sweeps were acquired under a given activation condition, i.e, pH and voltage. Clampfit was used to determine the mean and variance at any time point for the set of sweeps. The relationship between current variance and mean for a population of channels of discrete unitary current amplitude is defined by the following relationship:

$$\sigma^2(I) = i * I - I^2 / N, \quad (1)$$

with i, the single channel current, I, the mean current, and N, the number of channels in the patch (Sigworth, 1980). Thus, for a given $\sigma^2(I)$ vs. I plot (σ^2/I plot), not only can i and N be determined, but also the open probability (P_o) from $P_o(V, \text{pH}) = I_{max}/(i * N)$.

A difficulty in the application of this method is that, for channels that open to small values of P_o, N may not be well determined, such that estimates of P_o are also uncertain. Since Eq. 1 can be recast as $\sigma^2(I) = i*I(1 - P_o)$, for P_o is small (small values of mean current), $\sigma^2(I)$ z $i*I$. Thus, the initial slope of the σ^2/I relationship is essentially identical to i.

In the present work, we wished to make estimates of i, N, and P_o. However, even at pH 8.5 and +280 mV, the σ^2/I relationship exhibited only mild curvature, indicating that the channel open probability was <0.5. To evaluate the suitability of such datasets for estimates of N and P_o, variability in σ^2/I relationships was assessed through various simulation procedures (Lingle, 2006). This analysis indicated that, even with a set of 100 sweeps with a channel population of up to 1,000, there was considerable variability in estimates of N and P_o when the P_o value used for a simulation was 0.5 or less. However, more reliable estimates of N and P_o could be obtained even at low P_o, when multiple σ^2/I datasets from the same patch were fit simultaneously. This is equivalent to increasing the number of sweeps used for the σ^2/I determinations. Therefore, to better constrain our estimates of N and P_o, for each patch we obtained σ^2/I estimates over a range of voltages at both pH 8.5 and 7.6. The set of all σ^2/I estimates from a given patch (up to nine separate conditions in some cases; e.g., Fig. 4: 8 conditions) were then fit simultaneously with the following:

$$\sigma^2(I,V) = g * V * I - I^2 / N, \quad (2)$$

where the single channel conductance (g) times the command voltage defines the unitary current amplitude at a given potential. Simultaneous fitting of multiple σ^2/I relationships obtained from the same patch resulted in parameter estimates for P_o and i that exhibited marked agreement among all patches and with estimates from single channel measurements. Eq. 2 in essence assumes that the average single channel current varies in an ohmic fashion with voltage. Thus, the failure of Eq. 2 to describe σ^2/I relationships over a range of voltages would contradict the assumption that pH and voltage only affect P_o, but not g. As shown in Results, Eq. 2 holds for all σ^2/I relationships from a given patch, therefore yielding a constant and voltage-independent value of g.

For measurement of σ^2/I relationships at negative potentials, tail current variance was determined. Whereas at positive potentials i appears to vary linearly with voltage, this does not appear to be the case at negative potentials. To fit σ^2/I relationships at negative potentials, N was constrained to the value estimated from the preceding activation voltage step (either +280 or +240 mV) and i then determined. The first 200 μs of the tail current was omitted from this analysis.

An additional complication in the analysis of Slo3 σ^2/I relationships is that the single channel measurements suggest that individual Slo3 channels occupy either of two different conductance levels, O1 and O2, where O2 is ~50% of the main current level. In this case, is it justified to use Eq. 1 to fit the observed σ^2/I relationships? In Appendix, the predicted σ^2/I relationships are derived for a channel opening to either of two conductance levels where the fractional occupancy in the two levels is neither time nor voltage dependent. In this case, the expected σ^2/I relationship remains parabolic, and, dependent on the relative ratio of current amplitudes and fractional occupancies, the implications of the use of Eq. 1 for fitting the Slo3 σ^2/I relationships are given. Although the use of Eq. 1 to make an estimate of average i and P_o does result in errors, the magnitude of these errors does not compromise the key conclusions concerning limiting P_o that result from these experiments.

RESULTS

Macroscopic current at any condition reflects the number of channels (N) in a patch or cell, the elementary current (i) through an individual channel, and the probability that a channel is open (P_o) at a given condition. Since for most situations, N is invariant and, at least over some range of voltages, the elementary current varies ohmically with voltage, the macroscopic conductance (G) reflects solely the distribution of channels between closed and open states. Thus, $G(V) = N*g* P_o(V)$.

For Slo3 channels, increases in pH cause some shift in the G-V relationship to more negative potentials qualitatively similar to regulatory effects of Ca^{2+} on the homologous Slo1 K^+ channel (Zhang et al., 2006). However, the most dramatic effect of pH appears to be an increase in the apparent maximal conductance (g_{max}) of Slo3 macroscopic currents as pH is increased. This contrasts with Slo1 in which sufficiently positive

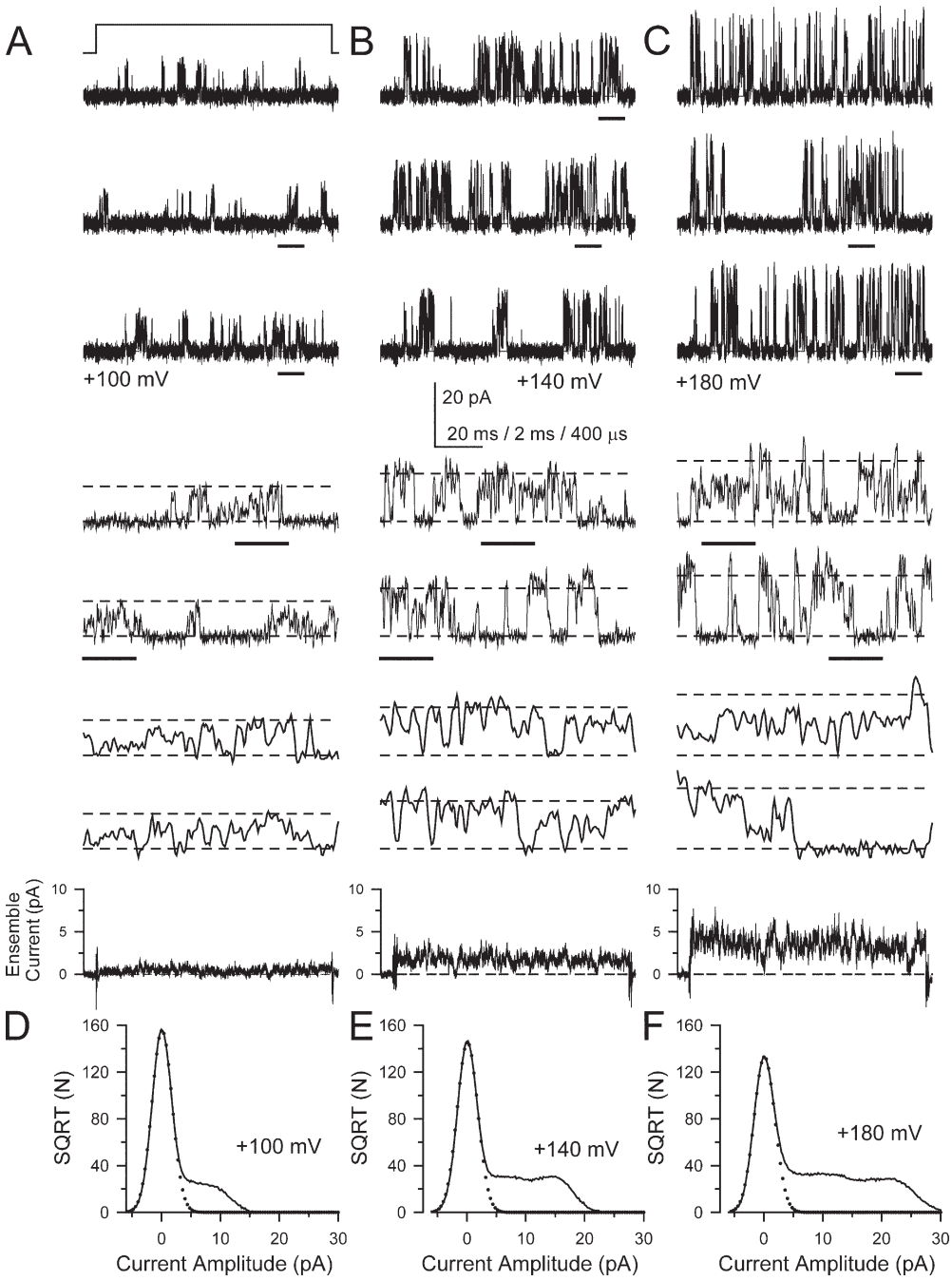

Figure 1. Single Slo3 channels exhibit complex open current level behavior. Slo3 channels were activated by repeated voltage steps to +100 (A), +140 (B), or +180 mV (C) from a holding potential of 0 mV. Example traces are shown at three different time bases. Horizontal bars under traces in A–C indicate segments of current displayed at a faster time-base below. Dotted lines on the expanded time-base segments indicate the 0 current level and the current level corresponding to a 110-pS single channel conductance. At the bottom of A–C, the average currents from sets of 40 sweeps are shown in each case, showing that a steady-state current level is rapidly achieved. Sample frequency, 100 kHz; filter, 10 kHz. pH 8.5. In D–F, histograms generated from all current values after the first 2 ms of each depolarizing step are shown. The time constant of macroscopic current activation at pH 8.5 over this voltage range is ~1 ms (Zhang et al., 2006). D–F also display the best fit (dotted line) of a Gaussian to the baseline current values. At both +140 and +180 mV, two clear maxima are observed in the open current levels. Each histogram was generated from a set of forty 100-ms sweeps.

activation potentials are able to drive Slo1 channels into similar saturating open probabilities (Cox et al., 1997), even at low [Ca^{2+}]. For Slo1, the similarity of the saturating P_o at different [Ca^{2+}] is expected to arise from the intrinsic voltage dependence of the closed–open equilibrium and the strength of coupling of voltage sensor movement to channel opening (Horrigan and Aldrich, 2002). For Slo3 channels, pH may exert effects on channel properties that are independent of effects on P_o, for example, by direct effects on ion permeation. Therefore, it is imperative that the effects of pH on Slo3 channel behavior be determined to establish the validity of the macroscopic measurements for mechanistic analysis.

Three particular properties of Slo3 single channels are of interest: first, the effect of pH and voltage on apparent single channel current amplitude, second, the single channel open probability (P_o) over the range of pH and voltages of the macroscopic current measurements, and, third, the maximal single channel P_o. To answer all of these questions would require the measurement of single channel activity at potentials positive to +200 mV. Because of the technical challenges to recording channel activity of sufficient duration at positive potentials,

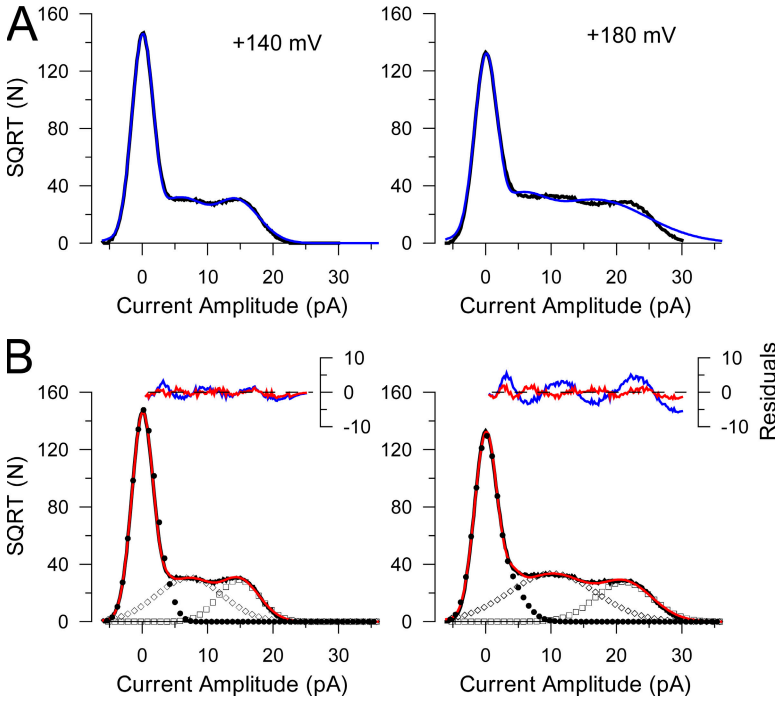

Figure 2. Open current levels can be approximated by two or three Gaussian components. In A, total amplitude histograms for currents activated at either +140 mV (left) or +180 mV (right) were fit (blue line) with three Gaussian components (one baseline and two open level components). At +180 mV the two open level components do not adequately describe the data. In B, the total amplitude histograms from A were fit with four Gaussian components (red line, one baseline and three open level components) and the individual Gaussian components are displayed (filled squares, sum of baseline and smallest open level component; open diamonds, open level 1; open squares, open level 2). The insets to each panel illustrate the residuals associated with the best fit for either the three (blue line) or four (red line) Gaussian fit. Although the four Gaussian fit better describes the data, the residuals are still not symmetrical around 0, indicative that a sum of Gaussian components does not fully describe the nature of these distributions.

we have approached this issue in two ways. First, we have made single channel measurements at potentials from +40 to +200 mV, a range over which substantial changes in macroscopic conductance are observed. Second, to obtain estimates of single channel behavior at potentials up to +300 mV, we have employed σ^2/I analysis.

Slo3 Channel Openings Exhibit Complex Open State Behaviors

For all results in this paper, Slo3 single channel activity or ensemble current activity at a given command potential was activated by repeated voltage steps usually of 200 ms duration. Examples of current openings at +100, +140, and +180 are shown for one patch in Fig. 1 (A–C). Activity was characterized by very brief openings and closings that preclude clear resolution of a well-defined open current level. Total amplitude histograms generated for a set of sweeps at the three command potentials reveal a complex distribution of current values (Fig. 1, D–F), suggestive of multiple current levels, each with rather substantial variance. The shape of the open current distributions was clearly not consistent with a simple filtering of a rapid two-state open to closed transition. The complexity in the open current behavior is also evident in the fastest time-base examples during which there is considerable variance in open current levels occurring on a time scale of tens to hundreds of milliseconds. Such variance in current levels is not found during complete closings of the Slo3 channel.

Total amplitude histograms were fit by a sum of Gaussian components. Visually, histograms from activity at the most positive voltages (positive to +100 mV) revealed two broad peaks in addition to baseline current values (Fig. 1, E and F). However, fits of three Gaussian components (Fig. 2 A; one baseline and two open levels), although adequate at the less positive potentials (e.g., +100 mV) did not adequately fit the histogram at the most positive voltages (e.g., +180 mV). Hence, over potentials of +120 to +180 mV, total amplitude histograms were best described by four Gaussian components (Fig. 2 B; three open levels and one baseline). Although a mean value for each of the open levels could be defined, each open level exhibited large variance that was relatively symmetric around the mean values. We have treated the smallest open level as a skewed shoulder in the baseline peak and have limited our analysis to the two primary open level components in the total amplitude histograms.

At Positive Potentials, Average Single Channel Current through Slo3 Channels Varies Ohmically with Voltage

For a set of four patches, the two open level components were measured for voltages of +120 through +180 mV. The mean amplitude of each component varied approximately ohmically with voltage (Fig. 3 A), yielding estimates of apparent mean conductance of 108.5 ± 5.1 pS (component O1) and 56.6 ± 1.7 pS (component O2). The relative contribution of each component to the distributions did not vary significantly with command voltage, and the smaller amplitude component (O2) contributed ~60% of all open current values (Fig. 3 B). The lack of change in the ratio of the two components indicates that voltage-dependent changes

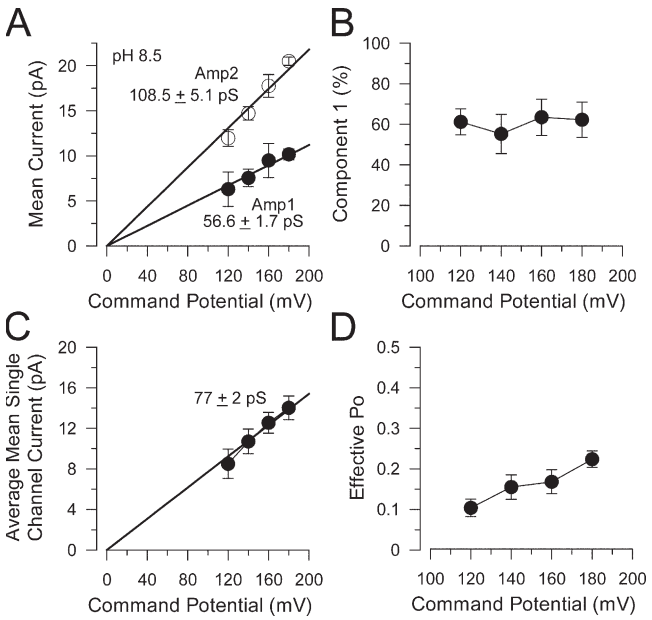

Figure 3. Empirical description of Slo3 open current amplitudes. In A, the mean amplitudes for the two largest components in the total amplitude histograms are plotted as a function of voltage for a set of four patches. Lines are the best fit through each set of points of $i = g^*V$, yielding conductance estimates of 108.5 ± 5.1 pS (O2) and 56.6 ± 1.7 pS (O1) for the two largest components of the histograms. In B, the total areas of components O1 and O2 was determined from histograms as in Fig. 2 and 100*O1/(O1 + O2) was calculated and plotted as a function of voltage. In C, average mean single channel current was determined from the areas and mean amplitude of O1 and O2, yielding an average single channel conductance of 77 ± 2 pS (mean ± 90% confidence limits). In D, an effective P_O at each voltage was calculated based on the fraction of time channels were either in O1 or O2.

in macroscopic Slo3 conductance do not arise from a voltage-dependent change in the fractional occupancy of the different conductance levels observed in the single channel behavior. Thus, at least over this limited voltage range, despite the complexity in the Slo3 behavior, the average mean current for a channel varies with voltage in an approximately ohmic fashion (Fig. 3 C). A weighted mean single channel current amplitude was defined based on both open level components, yielding an average single channel conductance of 77 ± 2 pS.

We next examined the effect of voltage on the fraction of time a Slo3 channel was in open states. From the total amplitude distributions, the fraction of time channels were in components O1 and O2 provides an estimate of the probability that a channel is in open states. P_o estimates made from the sum of the fractional time in O1 and O2 show that depolarization increases P_o, but that at +180 mV, channels are open only ∼20–25% of the time (Fig. 3 D).

The generally ohmic behavior of average Slo3 single channel current and absence of effects of voltage on the fraction of O1 and O2 provide some confidence that Slo3 macroscopic currents can be used to provide a description of the overall closed–open equilibrium behavior. However, this conclusion must be tempered because of the limited range over which such single channel properties were determined.

Average Unitary Currents of Slo3 Channels Vary Linearly with Voltage

To evaluate properties of Slo3 unitary currents over a wider range of activation conditions, we have employed analysis of Slo3 current variance. In Appendix, we derive and evaluate the predictions for σ^2/I relationships resulting from a population of channels in which individual channels can open into either of two conductance levels. In brief, the expected σ^2/I relationship remains parabolic. Furthermore, it is shown that for the case under consideration here, i.e., the single channel conductance of O2 is about half of O1, and the fractional occupancy within either open level is about the same, application of Eq. 1 will result in an estimate of apparent i that will exceed the average open channel current level estimated from single channel measurements by ∼10%. In addition, the estimate of P_o derived from application of Eq. 1 will systematically underestimate the true values by ∼10%. We therefore consider the estimates of i and P_o derived from application of Eq. 1 to Slo3 σ^2/I relationships as acceptable estimates of the underlying unitary behavior and that such estimates can be meaningfully compared with the direct single channel estimates described above.

The variance and mean of currents resulting from sets of 100 activation steps at a given voltage and pH were generated. For a set of 10 patches, σ^2/I relationships at any specified pH and voltage did not reveal any well-defined parabolic behavior. This suggests that the average P_o even at +280 mV and pH 8.5 was rather low, and well below 0.5. Based on the fact that increasing the number of sweeps used in the analysis helps improve reliability in the fitted estimates in σ^2/I analysis (Lingle, 2006), we used a strategy in which up to nine separate sets of σ^2/I relationships were simultaneously fit (Eq. 2) over voltages from +80 through +280 mV and including data at pH 8.5 (Fig. 4 A) and pH 7.6 (Fig. 4 B). From this procedure, estimates of unitary single channel conductance (g) and the number of Slo3 channels in the patch (N), were obtained for each patch. Over the range of voltages from +80 to +280 mV (Fig. 4 A; Fig. 5), the initial slope of the σ^2/I relationships was well described, indicating that the apparent single channel current does vary ohmically with voltage. Furthermore, this estimate of unitary conductance was similar at both pH 7.6 and pH 8.5 (Fig. 4 C), indicating that the effects of pH on macroscopic currents do not arise from an effect of pH on single channel current. For some patches, the σ^2/I relationship of binned mean current values (Steffan and Heinemann, 1997) was also determined

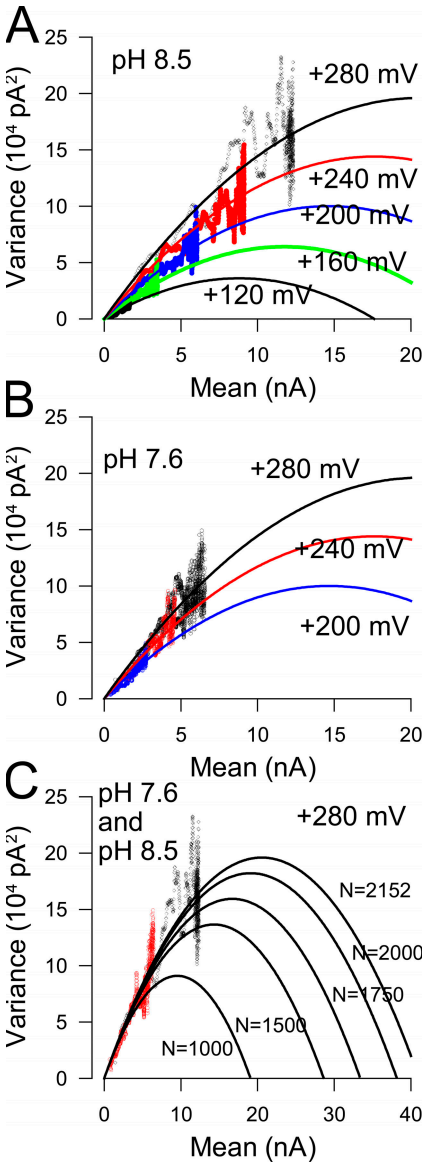

Figure 4. Analysis of Slo3 current variance allows estimates of g and N. In A and B, the current variance is plotted against mean currents for sets of 100 activation steps to five different voltages at pH 8.5 (A) and three different voltages at pH 7.6 (B), all from one patch. Each color corresponds to individual σ^2/I values at a different voltage as labeled on each panel. The activation step duration was 20 ms, sampled at 100 kHz, and filtered at 10 kHz. Lines are the best fit curves for Eq. 2 for each of the five voltages at pH 8.5. The fitted parameters were $g = 68.2 \pm 0.4$ pS (mean $\pm$ 90% c.l.) and $N = 2152.4 \pm 51.9$ channels. In C, the σ^2/I relationships for both pH 7.6 (red) and pH 8.5 (black) for +280 mV show that pH has no effect on the average single channel current (i). Lines show expected σ^2/I relationships for the indicated values of N with $i = 19.1$ pA. Values of $N \sim 20\%$ smaller than the best value result in parabolic relationships that clearly deviate from the observed σ^2/I values.

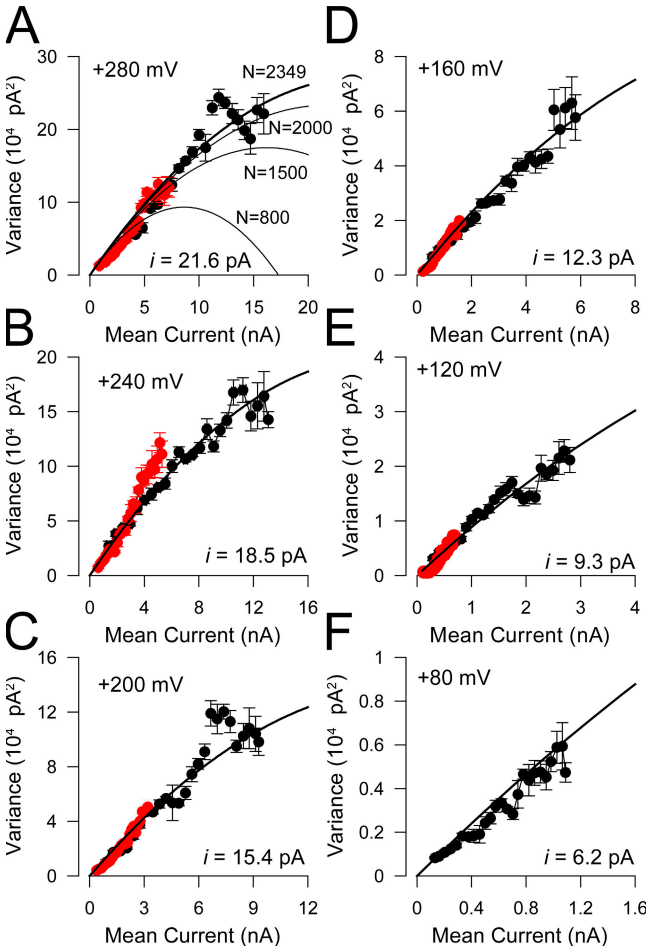

Figure 5. Binned σ^2/I data also indicate that Slo3 unitary current varies in an ohmic fashion. A–F display the average variance for sets of mean current values grouped into bins of identical width. Error bars indicate the standard deviation for the variance estimates in a given bin. For voltages from +120 through +280 mV, σ^2/I relationships are shown for both pH 8.5 (black) and pH 7.6 (red). The lack of effect of pH on the initial slope of the σ^2/I relationship indicates that pH has no direct effect on the average single channel current. Fitting Eq. 2 simultaneously to all the σ^2/I values (six voltages and two values of pH) yielded $g = 77.1 \pm 2.1$ pS and $N = 2349.5 \pm 302.8$ channels, resulting in the solid lines in each panel. In A, solid lines are also shown for $N = 2000$, $N = 1500$, and $N = 800$, indicating that smaller estimates of N (larger effective P_o) result in clear deviation from the observed data.

to minimize excess weighting by variance estimates where mean current is relatively unchanging (Fig. 5). Estimates using the binned σ^2/I approach were similar to those obtained using all mean current values.

After N was defined from the simultaneous fit of all σ^2/I relationships in a given patch, each individual σ^2/I relationship was then refit with N constrained to the value defined from the simultaneous fit. This provided individual estimates of i at different voltages and pH (Fig. 6), yielding single channel estimates of 81 $\pm$ 2 pS for all patches at pH 8.5 and 76 $\pm$ 16 pS for all patches at pH 7.6. Consistent with the direct unitary current measurements from single channel patches (Fig. 6, red circles), the average unitary current estimate from σ^2/I analysis varied ohmically over the range of +80 to +280 mV. The conductance estimates from σ^2/I analysis are

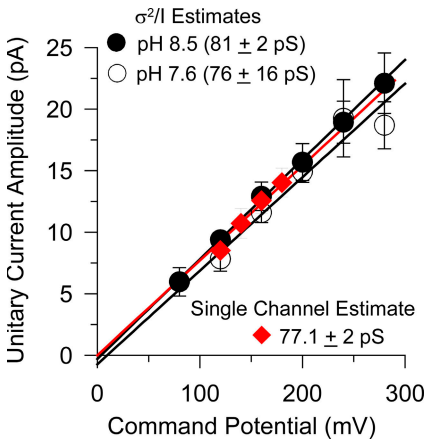

Figure 6. The dependence of Slo3 unitary current amplitude on voltage. Estimates of the unitary current amplitude from σ^2/I analysis are plotted as a function of voltage for both pH 8.5 and pH 7.6. Individual estimates at each voltage were obtained as described in the text. For comparison, red symbols correspond to average unitary current estimates from single channel measurements. Lines correspond to the best fit of $i(V) = g^*V - b$.

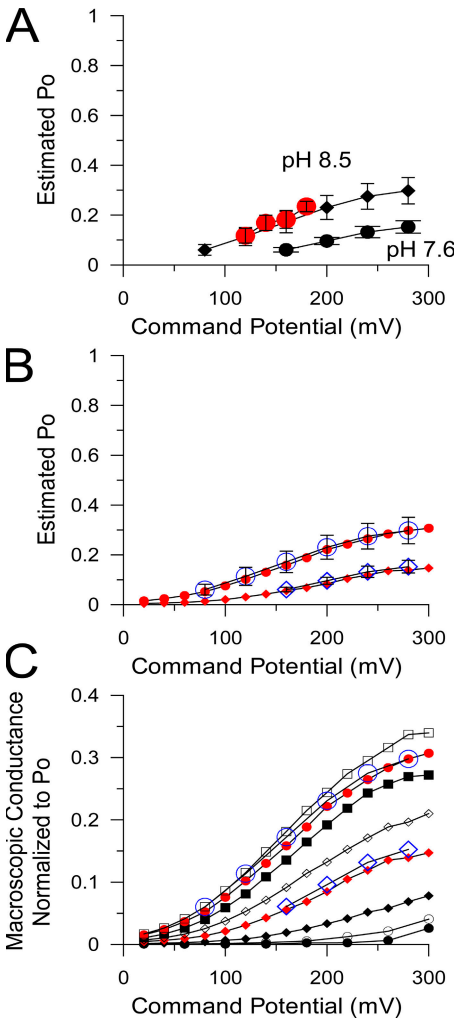

Figure 7. The pH and voltage dependence of Slo3 Po. In A, values of N obtained from fitting families of σ^2/I relationships were used to define the estimated P_o at different pH and voltage. P_o was defined for eight patches at pH 8.5 (filled diamonds), for which N was defined from simultaneous fit of at least five different σ^2/I relationships. For five of those patches, P_o was also determined for four voltages at pH 7.6 (filled circles). Error bars correspond to SD. For comparison estimates of P_o at pH 8.5 based on single channel current measurements are included (red circles). In B, the macroscopic G-V curves for Slo3 activation at pH 8.5 (red circles) and 7.6 (red diamonds) were normalized to the unitary current P_o estimates in A (blue symbols) by setting the macroscopic conductance estimate at pH 8.5 and +280 mV identical to the unitary current estimate at the same condition. In C, following the procedure used in B, all macroscopic conductance values at pH of 6.0, 7.0, 7.4, 7.6, 7.8, 8.0, 8.5, and 9.0 (Zhang et al., 2006) were normalized to absolute P_o estimates. Blue symbols represent estimates from σ^2/I analysis as in A.

therefore quite similar to the average single channel current estimates from single channel experiments. Based on the considerations given in the Appendix, we would have expected the apparent estimate of i from the σ^2/I to exceed the weighted mean of the single channel current amplitudes by ~10%. Given the nature of each type of measurement and the procedures used to extract the average unitary current values, we simply view the results as support for the idea that both methods are yielding similar information about the unitary current properties. The key point of significance for our understanding of Slo3 gating behavior is that the estimates of unitary current from the σ^2/I method vary ohmically with voltage and are not influenced by pH. At pH 8.5, our results strongly argue that the relative occupancy of channels in O1 and O2 open levels is not influenced by either voltage or pH. At pH 7.6, we do not have direct measurements of fractional occupancy in O1 and O2. However, based on the considerations in the Appendix and the fact that the unitary current estimates from the σ^2/I method are identical at both pH, a pH-dependent change in fractional occupancy of O1 and O2 would require that the ratio of the amplitudes I1 and I2 was also changing. A simpler explanation for the equivalence of the σ^2/I estimates of single channel current at both pH 7.6 and 8.5 is that fractional occupancy in O1 and O2 is not influenced by pH.

Slo3 Open Probability Is Increased by Both Depolarization and Increases in pH

The estimated values for i and N for a given patch were used to calculate P_o ($P_o = I_{max}/i^*N$) at each voltage and pH. At pH 8.5 and +280 mV, the maximal P_o was ~0.3 (Fig. 7 A), suggesting that the limiting P_o for Slo3 channels is quite low compared with Slo1 channels. As developed in Appendix, these estimates are expected to be on the order of ~10% less than the true P_o, a deviation certainly within the variability among patches. Is it possible that the estimates of P_o by this method are severe underestimates? This seems highly unlikely since if the true P_o was substantially higher, it would require that the

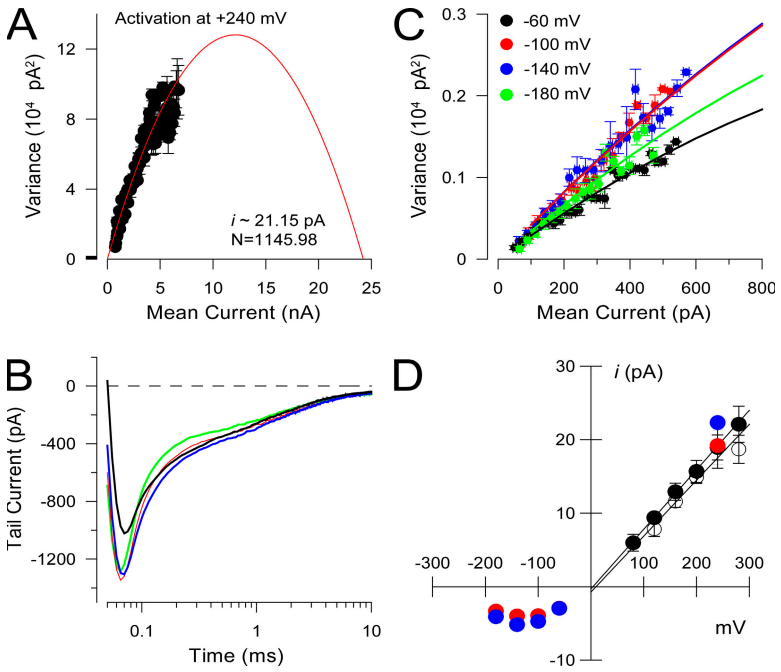

Figure 8. Nonohmic behavior of tail current amplitude at negative potentials is associated with nonohmic reductions in apparent average single channel current amplitude. In A, binned σ^2/I relationships for four sets of 100 steps to +240 mV are displayed along with the best fit of Eq. 1 with i = 21.15 pA; N = 1146. In B, the tail currents (10 kHz filtering) after repolarization to −60 (black), −100 (red), −140 (blue), and −180 (green) mV from the initial step to +240 mV are shown on a logarithmic time base to emphasize the two exponential nature of the tail current decay. The peak of the tail current is essentially unchanged between −100 and −180 mV. In C, the binned σ^2/I relationships for each of the tail currents shown in B are shown. N was constrained to the value obtained in B (N = 1146) and i obtained from the fit of Eq. 1. Apparent single channel current amplitude does not increase at potentials more negative than −100 mV, despite the increase in driving force. In D, the estimated i from examples like that in C are plotted as a function of voltage (red symbols), along with the estimates of i obtained from σ^2/I analysis at positive potentials. Blue symbols correspond to records filtered at 50 kHz and red symbols to those filtered at 10 kHz.

σ^2/I relationships should show substantially more curvature. As illustrated (Fig. 4 C and Fig. 5 A), a higher P_o (than estimated) requires that N be smaller than what we have observed. A decrease in the estimate of N on the order of 25% results in σ^2/I relationships that are clearly inconsistent with the observed data. On the other hand, it is more difficult to exclude the possibility that we are overestimating the true P_o, since the observed σ^2/I relationships reveal only a slight curvature. Irrespective of this uncertainty, the results clearly argue that the limiting Slo3 open probability even at pH 8.5 and +280 mV probably does not exceed 0.3. Furthermore, irrespective of the actual limiting values at +280 mV, the limiting values do differ between pH 8.5 and pH 7.6, since these estimates are defined within the same patch. P_o estimates from the σ^2/I analysis are summarized in Fig. 7 A with P_o estimates from the unitary single channel current analysis also included for comparison. Both procedures provide essentially identical estimates for single channel P_o.

To compare the voltage dependence of Slo3 P_o to the macroscopic Slo3 conductance, the value of the macroscopic conductance at pH 8.5 and +280 mV was normalized to the σ^2/I estimate of P_o at pH 8.5 and +280 mV (Fig. 7 B). This normalization procedure shows that the dependence of Slo3 single channel P_o at pH 7.6 and 8.5 follows a similar dependence on voltage and pH as the macroscopic conductance estimates. Similarly, using all macroscopic conductance values, the complete dependence of Slo3 Po on voltage and pH is shown in Fig. 7 C. Overall, this analysis supports the view that the limiting P_o at positive potentials differs at different pH.

Reduced Apparent Single Channel Amplitudes at Negative Potentials Probably Arises from Effects of Filtering on a Fast Channel Closing Process

Macroscopic recordings show that Slo3 currents deactivate very rapidly at negative potentials such that the peak of the Slo3 tail current exhibits a markedly nonohmic behavior (Zhang et al., 2006). In fact, peak tail current amplitude measured at 10 kHz bandwidth is essentially flat from −80 through −200 mV, despite the over twofold increase in driving force on the currents.

We examined the properties of unitary Slo3 currents under similar conditions by undertaking an analysis of Slo3 current variance during tail currents. Currents were initially activated by repeated steps to +240 mV and then tail currents monitored at potentials of −60, −100, −140, or −180 mV (Fig. 8 B). From the averages of four sets of currents, an estimate of N was obtained from the fit of the binned σ^2/I relationship at +240 mV (Fig. 8 A). The σ^2/I relationships at each negative voltage were then fit (Fig. 8 C) with N constrained to the value estimated at +240 mV. Although the estimate of i at −60 mV was essentially ohmic with the estimate at positive potentials, at more negative potentials, the estimate of i showed marked rectification (Fig. 8 D). If this nonlinearity in Slo3 single channel conductance reflects a true change in conductance rather than a consequence of filtering of rapid kinetic transitions underlying Slo3 gating equilibria, this would cause errors in attempts to estimate Slo3 conductance at negative potentials.

We have therefore evaluated the extent to which the reductions in tail current amplitude and estimates of single channel current amplitudes are predicted by the

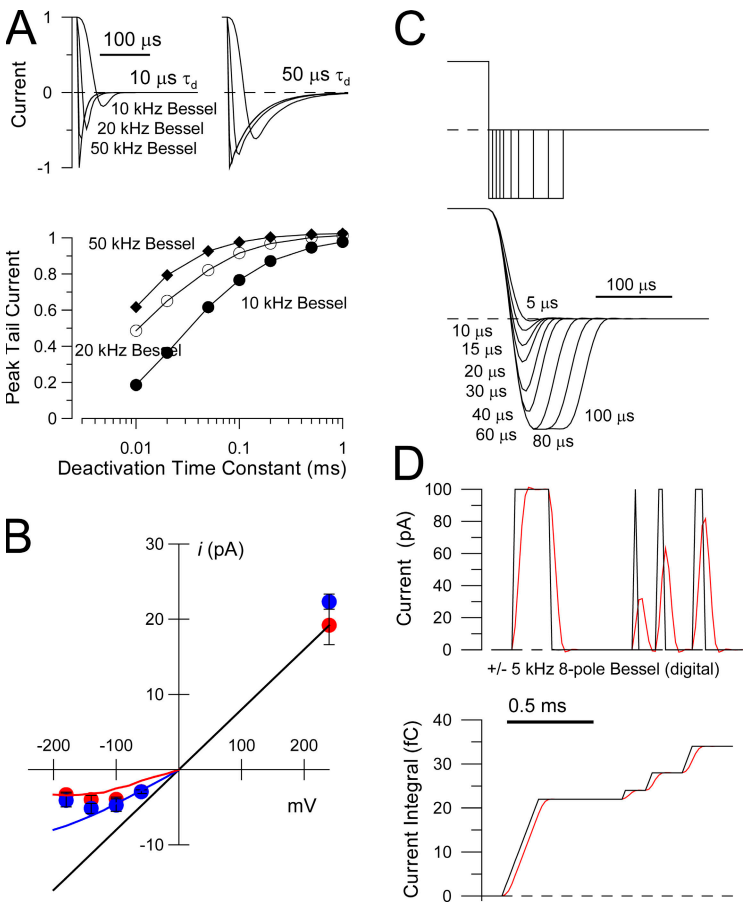

Figure 9. Filtering accounts for apparent reductions in single channel current amplitude, but does not compromise estimates of net current flux. In A, tail currents decaying with deactivation time constants (τ_d) of either 10 (left) or 50 µs were simulated and digitally filtered with 10, 20, or 50 kHz 8-pole Bessel filter settings. In the bottom panel, peak tail current amplitude as a function of τ_d is plotted at different filter settings. In B, the theoretical reduction of peak tail current determined from simulations as in A based on measured Slo3 τ_d values (blue line, 50 kHz Bessel; red line, 10 kHz Bessel) are compared with the single channel estimates from σ^2/I analysis (10 kHz, red circles; 50 kHz, blue circles; Fig. 8 D). Tail current amplitude estimates were normalized to the single channel current amplitude at +240 mV. Solid black line shows a strictly ohmic relationship. In C, the impact of filtering (10 kHz) on idealized single channel closures (top traces) after repolarization is illustrated. After the time of repolarization, examples show channels closing at times ranging from 5 to 100 µs. With 10 kHz filtering, channels closing in <20 µs would be barely detectable based on half-amplitude detection. In D, the effect of filtering on detection of average current is shown. On the top, idealized single channel openings are shown either without or with (red line) 5 kHz filtering. On the bottom, the total charge passing through channels in the two cases is compared showing that filtering does not reduce the total current arising from any individual channel opening.

filtering levels used in our experiments. Fig. 9 A examines the reduction in idealized tail current amplitude at a given voltage that would be expected based on different deactivation time constants (τ_d: 10, 20, and 50 µs) and filtering settings (10, 20, and 50 kHz 8-pole Bessel). With τ_d = 50 µs, marked reduction of tail current amplitude is observed at both 10 and 20 kHz filtering, while at τ_d = 10 µs, even the 50 kHz filtering reduces peak tail current by almost 40%. For comparison, the major component of Slo3 deactivation is ~15–30 µs, becoming somewhat faster at more negative potentials. The typical filtering used in our experiments was 10 kHz. Based on the measured τ_d for Slo3 over voltages of −60 to −200 mV, the relationships developed in Fig. 9 A allow a calculation of the fractional reduction in tail current amplitude expected for the measured Slo3 τ_d estimates. This predicted fractional reduction both for 10 and 50 kHz is compared with the measured estimates of single channel current (from σ^2/I analysis; Fig. 8 D) at both 10 and 50 kHz (Fig. 9 B). The nonlinearity in the single channel current estimates generally approximates the expected reduction in tail current amplitude. Similarly, 10 kHz filtering of idealized single channel closures following a voltage step shows that for openings lasting <30 µs, the observed single channel amplitude will be markedly reduced (Fig. 9 C). This suggests that the σ^2/I estimate of single channel current at negative potentials represents the average open channel current level from largely unresolved openings, and not a true reduction in single channel current amplitude.

These considerations argue that the flattening of the single channel current estimates at negative potentials represents the rapidity of the underlying Slo3 gating mechanisms and not a true effect on conductance. Since the intrinsic value of single channel conductance does not vary with voltage, the net charge through Slo3 channels at negative potentials should therefore provide a direct measure of the gating equilibrium–dependent open probability at those potentials, irrespective of the effects of filtering. This is summarized in Fig. 9 D, in which it is shown that the net charge through any open channel is unaffected by filtering, no matter how brief the opening.

Slo3 Channel P_o at Negative Potentials Is Appreciable and Relatively Voltage Independent

Macroscopic measurements suggest that Slo3 conductance at negative potentials and pH 8.5 may be ~0.1–1% of the Slo3 conductance at positive potentials and be relatively voltage independent (Zhang et al., 2006). Here in patches with very few channels, we examine Slo3 channel activity at negative potentials. A primary

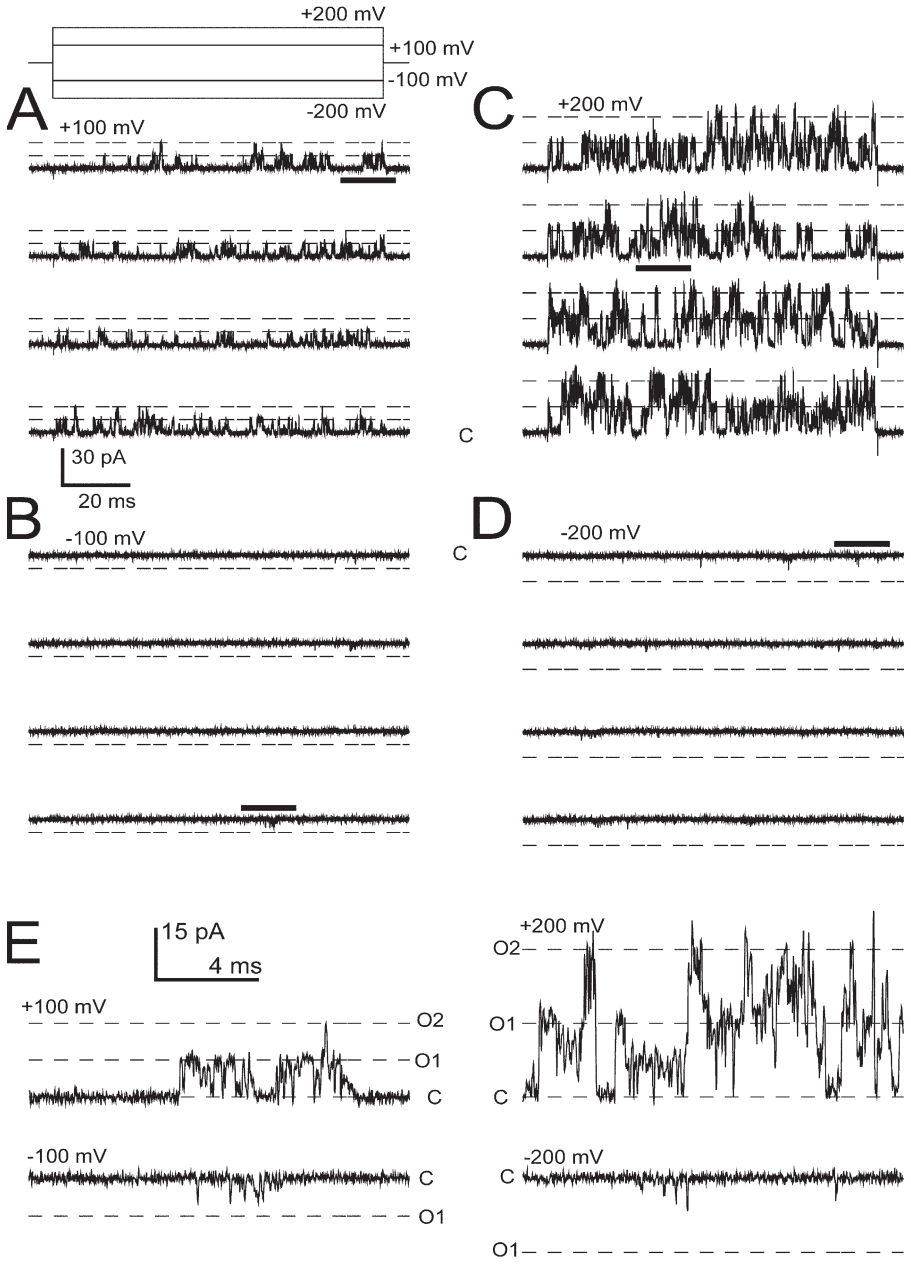

Figure 10. Openings of Slo3 channels at positive and negative potentials. Channels were activated by voltage steps to potentials of +100 (A), −100 (B), +200 (C), and −200 (D) mV from a holding potential of 0 mV. Dotted lines correspond to the expected current level for the maximal open level component for one (110 pS; Figs. 2 and 3) or two open (220 pS) channels. Brief, small amplitude openings are observed at −100 and −200 mV. 10 kHz filtering. Horizontal lines above or below traces in panels A–D define segments shown at expanded time base in E. C, O1, and O2 correspond to the closed current level and the 110 pS level for one (O1) or two open channels (O2).

difficulty in these experiments is that the brief and flickery nature of the Slo3 channel openings make it difficult to assert unambiguously whether particular events are, in fact, Slo3 openings. However, such pH-dependent activity is not observed in patches from DEPC-injected ($n = 3$) or uninjected ($n = 2$) oocytes. As a consequence, here for the moment we simply assume that the events we see observed are Slo3 openings. We then ask whether the observed events have properties we might expect for Slo3 openings.

Examples of Slo3 channel activity in a two-channel patch are shown for each of four potentials (+100 mV, Fig. 10 A; −100 mV, Fig. 10 B; +200 mV, Fig. 10 C; −200 mV, Fig. 10 D). A clear increase in channel P_o is seen in moving from −100 to +100 mV and then to +200 mV. Whereas the openings to the largest conductance level expected for a single channel (O1: 110 pS) exhibit a generally ohmic behavior at +100 mV and +200 mV, the brief open events at −100 and −200 mV fail to approach the 110 pS level. Based on rapid deactivation at negative potentials and the effect of filtering, the brevity and amplitude of these events are not unexpected. Faster time-base examples of activity at each of these four potentials is shown in Fig. 10 (E and F). The less than ohmic peak amplitudes of the brief events at negative potentials are generally consistent with the reductions seen in unitary current amplitudes from the σ^2/I analysis of the tail currents (Figs. 8 and 9).

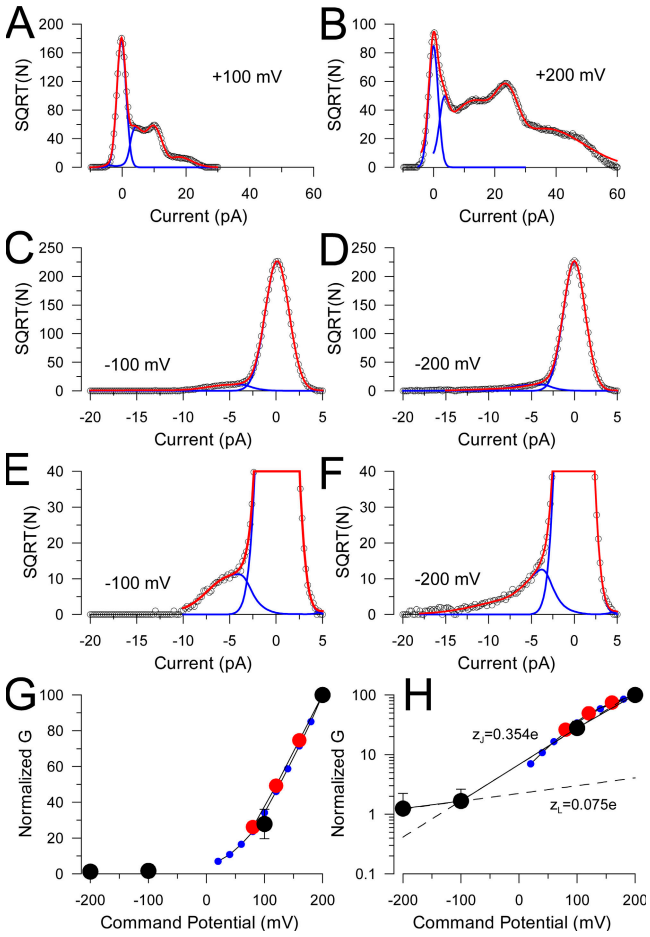

Figure 11. Comparison of total amplitude histograms at positive and negative potentials reveals that Slo3 conductance at pH 8.5 is appreciable at negative potentials. In A–D, total amplitude histograms for traces from the patch in Fig. 9 were generated for each of four voltages and fit with some number of Gaussian components. In E and F, histograms for currents at −100 and −200 mV were rescaled to emphasize the open channel activity. In G, the average current during all sweeps at a given voltage were converted into a conductance normalized to the value at +200 mV (black circles). For comparison, normalized macroscopic conductance (blue circles) and P_o estimated from σ^2/I measurements (red circles) are overlaid. In H, log(G) is plotted as a function of voltage. Lines represent limiting slope fits of $G(V) = G(0)$*exp(zFV/RT) for the two most negative voltages (−200 and −100 mV, $z_L \sim 0.075$ e) and the three most positive voltages (−100–200 mV, $z_J \sim 0.354$ e).

To make estimates of relative conductance for such patches, total amplitude histograms for all traces at a given voltage were generated (Fig. 11, A–F) with care taken to ensure that the bins corresponding to the fully closed channels were symmetrically distributed around 0 current. For all current values, the average current in excess of the baseline was then determined for each voltage. From this, the average conductance at each voltage was calculated (Fig. 11, G and H). The results from this analysis indicate that the brief Slo3 openings observed at −100 and −200 mV at pH 8.5 contribute a total conductance that is approximately two to three orders of magnitude less than that observed at the most positive activation potentials. Although stochastic variability is most certainly an issue in such patches, any change in the measured conductance between −100 and −200 mV appears minimal compared with changes observed between −100 and +200 mV. A fit to the points at −100 and −200 yields an estimate of the voltage dependence of the closed–open equilibrium of 0.075 e. For the points at −100, +100, and +200 mV, the fitted slope yields an effective valence of 0.354 e, presumably reflecting primarily the contributions of voltage sensor equilibrium to current activation.

In the absence of established pharmacological tools to block Slo3 channels, it is difficult to prove that the brief events seen at negative potentials are unquestionably Slo3 openings. Yet, the observed openings have the reduced amplitude and rapid kinetic behavior expected for Slo3 openings, and also contribute to the overall conductance in a way that is consistent with our expectations from other measurements. Thus, it seems likely that the events we are observing at −100 and −200 mV are Slo3 openings.

As an additional test of the properties of unitary Slo3 openings at negative potentials, we have examined single channel tail currents conditional on an opening occurring at the end of a preceding depolarizing step. Leak and uncompensated capacitance were removed using an idealization of an adjacent null sweep. For two patches, tail current openings were monitored at either −80 or −100 mV. A set of 60 traces was identified in which both an opening occurred at the end of the depolarization and an adjacent sweep contained no openings. After subtraction, 22 of the 60 openings revealed clear tail current openings that closed in much less than 1 ms. This frequency of detected closures fits closely with the expectation for channels closing at a rate approaching 50 kHz with 10 kHz filtering (Fig. 9 C). Most closures would simply not be detected, since closure would occur during the transition from outward to inward current. Selected examples of cases in which such openings were observed are shown in Fig. 12. These tail current closures of Slo3 channels are qualitatively similar in terms of brevity and amplitude to the openings seen at −100 mV in Fig. 10. In rare cases, similar reopenings are also observed (e.g., Fig. 12, third trace from top) at later times in the trace. These observations lend support to the idea that the measured steady-state channel activity examined in Fig. 11 does, in fact, reflect Slo3 channels.

DISCUSSION

Despite the complexity observed in the amplitudes and kinetic behavior of Slo3 channel openings, the results described here support the simple conclusion that the

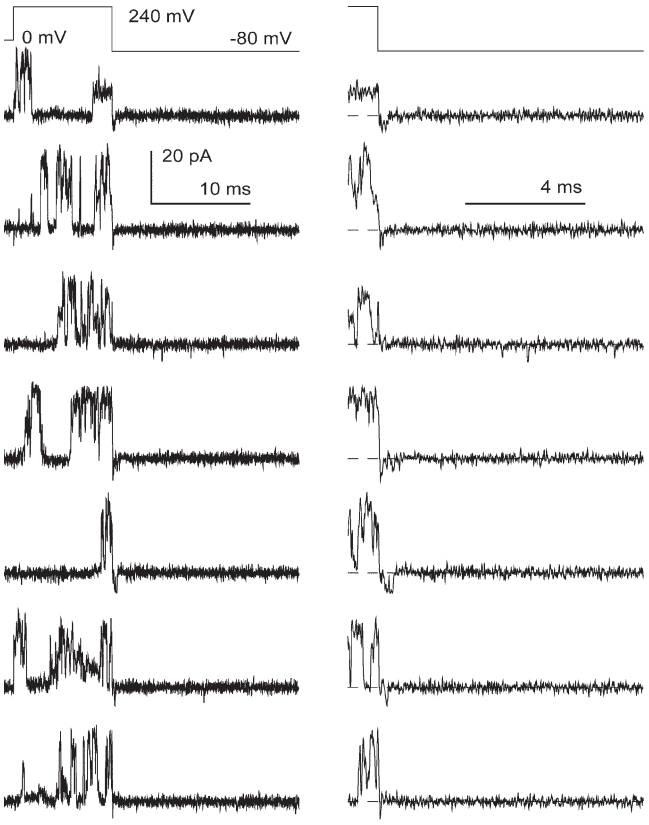

Figure 12. Tails of Slo3 channel openings after repolarization. Slo3 openings at pH 8.5 in a single channel patch were activated by 10-ms depolarizations to +240 mV from a holding potential of 0 mV, with a subsequent repolarizing step to −80 mV. Sweeps either immediately preceding or following a sweep with an opening at the end of the 10-ms step were used for subtraction of uncompensated C_m and leak. Traces on the right show the tail openings for the traces on the left at a faster time base. Sample traces were selected to emphasize the openings and closures after repolarization, except in the case of the third trace from the top. On average, tail openings were not observed in over half of those sweeps in which a Slo3 channel was active at the end of the depolarization.

average current during openings of Slo3 channels behaves in a typical fashion. Namely, the average single channel current amplitude varies in an ohmic fashion with voltage. Furthermore, pH in the range that activates Slo3 currents has no direct effect on the average single channel current amplitude. Coupled with estimates of the P_o of Slo3 channels at different voltages and pH, the results also indicate that the limiting P_o estimates at the highest command potentials are quite small compared with similar measurements in Slo1. In addition, consistent with macroscopic current measurements (Zhang et al., 2006), the limiting P_o appears to be pH dependent. Finally, estimates of Slo3 conductance at negative potentials in patches with just a few channels are generally consistent with macroscopic current measurements. Specifically, Slo3 conductance at negative potentials is relatively voltage independent and, at pH 8.5, Slo3 conductance is only approximately two to three orders of magnitude less than the conductance at the most positive activation potentials. Thus, these results provide assurance that the pH dependence of macroscopic currents reflects pH-dependent regulatory effects on conformational equilibria and not direct effects of pH on ion channel permeation (Zhang et al., 2006).

The implications of these properties of Slo3 currents in terms of the mechanisms of allosteric regulation are developed more fully in the associated paper (Zhang et al., 2006), but one key conclusion is summarized here. Specifically, both macroscopic and unitary current measurements argue that the behavior of the limiting Slo3 conductance at both positive and negative potentials differs markedly from Slo1 (Horrigan and Aldrich, 2002). Slo3 exhibits a pH-dependent maximum conductance at positive potentials and a relatively voltage-independent conductance at negative potentials. In contrast, for Slo1, the limiting conductance at positive potentials is relatively independent of $[Ca^{2+}]$, while at negative potentials, the residual voltage dependence of P_o is greater in Slo1 (Horrigan and Aldrich, 2002) than Slo3 (Zhang et al., 2006). This difference between Slo1 and Slo3 both at more positive potentials and more negative potentials can be largely explained if the closed–open equilibrium (L) for the Slo3 channel has a much smaller voltage dependence ($z_L \sim 0.04$) compared with Slo1 ($z_L \sim 0.3$). This was, in fact, observed in the single channel measurements in Figs. 10 and 11 here and also supported by macroscopic current measurements (Zhang et al., 2006). In addition, the difference (100–500-fold) in Slo3 P_o at the extremes of potentials seems somewhat less than observed for Slo1, where at 100 μM Ca^{2+}, P_o varies 1,000–5,000-fold at extremes of voltage (Horrigan and Aldrich, 2002) and $>10^6$-fold at low Ca^{2+}. This suggests that voltage sensor movement is more weakly coupled to channel opening in Slo3 than in Slo1, and this point is more fully supported with macroscopic current measurements (Zhang et al., 2006).

In sum, then, the current results support the simple but essential assertion that changes in macroscopic Slo3 conductance represent solely pH and voltage-dependent changes in single channel P_o.

The Large Variance in Open Current Levels of Single Slo3 Channels

Despite the fact that the average Slo3 single channel current can be considered well behaved in the sense that the relationship $G(V, \text{pH}) = N*g*P_o(V, \text{pH})$ is applicable, it is also true that Slo3 exhibits complex rapid opening and closing behavior quite distinct from its more staid kin, Slo1. By this we are referring to the point-to-point current variance during open channels that greatly exceeds the baseline variance (Fig. 1).

Specifically, Slo3 single channel openings do not exhibit well-defined current levels and the variance around

either of the two average open levels is large on the time scale of tens to hundreds of microseconds. This is markedly different from Slo1, for which relatively stable open levels are observed. Slo3 currents have been reported to have a relatively high permeability to Na^+ (Schreiber et al., 1998), suggesting that intrinsic ion permeation properties may differ between Slo1 and Slo3 perhaps related to the differences in conductance. One notable difference between Slo1 and Slo3 is that in Slo1, the key selectivity filter sequence is GYGD, whereas it is GFGD in Slo3. However, the F/Y mutation in Slo3 does not produce any obvious changes in the single channel conductance or variance in open current levels (unpublished data). The basis for the differences in apparent single channel conductance and open channel gating behavior between Slo1 and Slo3 remains an interesting topic for future investigation.

APPENDIX

σ^2 as a Function of Mean Current for a Channel with Two Conductance Levels

The relationship for variance (σ^2) as a function of mean current, I, resulting from a population of N channels with single channel current, i, is given by (Sigworth, 1980)

$$\sigma^2 = iI - \frac{I^2}{N}. \tag{1}$$

Guided by a derivation for Eq. 1 (Hille, 2001), here we derive a similar relationship for a population of N channels that can open to either of two open current levels, i_1 and i_2. We assume that the equilibrium between occupancy in i_1 and i_2 is voltage independent, such that under all conditions, $p(i_2)/p(i_1) = k$, i.e., the ratio of the probabilities of a channel being in either open level is constant (k). Given that for Slo3 single channel current openings, the ratio of the two open amplitude components is constant at all voltages, this assumption seems appropriate.

The standard expression for variance of a series of observations is

$$\sigma_x^2 = \frac{1}{n}\sum_{j=1}^{n}(x_j - \bar{x})^2. \tag{2}$$

After expansion of the quadratic and, noting that $\sum x_i / n = \bar{x}$, simplification leads to

$$\sigma_x^2 = \left(\frac{1}{n}\sum_{i=1}^{n} x_i^2\right) - \bar{x}^2. \tag{3}$$

For a single channel that opens to either of two levels, i_1 and i_2, with fractional probabilities p_1 and p_2,

$$\bar{x} = p_1 i_1 + p_2 i_2. \tag{4}$$

The mean squared current for n observations of the single channel current amplitudes is given by

$$\frac{\sum x_i^2}{n_T} = (n_1 i_1^2 + n_2 i_2^2)/n_T = p_1 i_1^2 + p_2 i_2^2. \tag{5}$$

Substituting the expressions in Eqs. 4 and 5 into Eq. 3 and remembering that $p_2/p_1 = k$ yields

$$\sigma^2 = p_1 i_1^{\,2} + k p_1 i_2^{\,2} - (p_1 i_1 + k p_1 i_2)^2. \tag{6}$$

For a population of N independent channels with two conductances, the mean current I is

$$I = N(p_1 i_1 + k p_1 i_2) = N p_1 (i_1 + k i_2). \tag{7}$$

Since the variance from each channel is additive, Eq. 6 yields

$$\sigma^2 = N p_1 (i_1^{\,2} + k i_2^{\,2}) - N(p_1 i_1 + k p_1 i_2)^2. \tag{8}$$

Then, combining Eq. 7 with 8 produces

$$\sigma^2 = I\frac{i_1^{\,2} + k i_2^{\,2}}{i_1 + k i_2} - \frac{I^2}{N}. \tag{9}$$

Eq. 9 is identical in form to Eq. 1 for the variance resulting from the population of N channels opening to a single amplitude level. Thus, for a channel opening to two conductance levels, the predicted relationship between σ^2 and I will be parabolic for the case that the ratio of time in the two conductance levels is always constant. When the ratio of time in different conductance levels changes with time, the shape of the σ^2/I relationship will depend in a complicated way on the changing ratio of occupancy of the different open states. Similarly, changes in the ratio of occupancy with ligand or voltage will preclude simple comparison of changes in the σ^2/I relationship under different conditions.

Using Eq. 9, we have examined the theoretical expectations for a population of 1,000 channels, with $i_1 = 20$ pA, and i_2 varying between 0 and 17.5 pA (Fig. A1, A). In this case, $k = 1$, i.e., each channel is equally likely to be in either i_1 or i_2. In each case, as i_2 is varied, the resulting relationship is parabolic with an empirical I_{max} given by $500*i_1 + 500*i_2$, denoted for each i_2 by the symbol at the rightmost end of each parabola. In each case, a fit of the standard expression for the σ^2/I relationship (Eq. 1) yields an estimate of apparent N' and i'. In each case, N was 1,000 while the estimates of i' reached a minimum of ~82% of i_1 (Fig. A1, B.) The time-averaged estimate of average single channel current amplitude based on i_1 and i_2 is shown for comparison (Fig. A1, B) and varies linearly over the range of possible estimates for i_2. Thus, for N channels that are equally likely to be in either of two open current levels (10 and 20 pA), the initial slope of the σ^2/I relationship yields an empirical

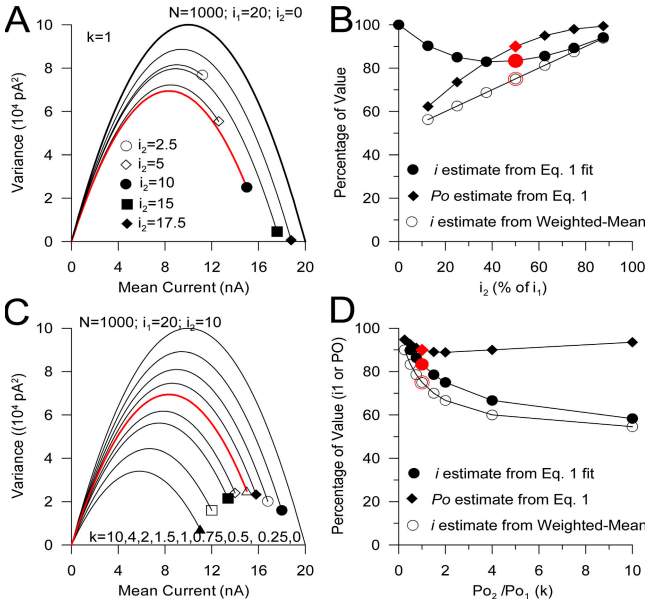

Figure A1. σ^2 estimates of single channel properties for channels with two conductance levels. In A, predicted σ^2/I relationships for a population of 1,000 channels in which each channel can occupy a main conductance level (i_1) of 20 units and a second level, i_2, as indicated. Fractional occupancy in each level is 0.5. In each case, a parabolic relationship is expected, but the maximal possible value of I when all channels are open depends on the relative amplitudes of i_1 and i_2. The curve in red approximates the expectation based on the single channel properties of Slo3. In B, the values of i (solid circles) and P_o (diamonds) based on applying Eq. 1 to the parabolas in A are given for different values of i_2. For estimates of i, the estimated value is given as a percentage of the nominal value of i_1, while, for P_o, the value given is the percentage by which the apparent P_o defined from application of Eq. 1 will underestimate the true P_o. For comparison, the weighted-mean estimate of single channel current based on the relative amplitudes and fractional occupancy in each of two open states based on amplitude histograms is given (open circles). For the case applicable to Slo3 (red symbols), i estimated using Eq. 1 will be within 10% of the weighted-mean estimate of average single channel current, while the P_o estimate will underestimate the true P_o by ~10%. In C, the impact of changing the relative occupancy, k, in i_2 and i_1 is considered, while in D, the impact of k on parameter estimates using Eq. 1 are shown.

estimate of the apparent single channel current of 16.667 pA, while the weighted mean for the two levels would be 15 pA. When i_2 is small relative to i_1, the difference between i_2 and i_1 becomes a bigger contributor to the σ^2, such that the initial slope of the σ^2/I relationship again begins to approach i_1.

This analysis indicates the following. First, for channels with multiple conductance levels, the σ^2/I relationship is expected to be parabolic. Second, although the apparent elementary conductance estimated from Eq. 1 has no exact significance, when $i_2 \geq \sim 0.5 i_1$, the initial slope of the σ^2/I relationship is only somewhat greater than the weighted mean of open channel current amplitudes estimated from total amplitude histograms. Third, in the situation that channels only occupy open states, which is the condition of maximal activation, the σ^2 remains appreciable. If a single open channel current level is assumed, such curves would then have the effect of underestimating the apparent open probability of the channels, since maximal current is reached when variance is still appreciable (end points for parabolas in Fig. A1, A). For cases when i_2 is $\geq \sim 0.5 i_1$, the magnitude of this error would not be very large (filled diamonds in Fig. A1, B).

We also evaluated the effect of changing the constant, k (Fig. A1, C). In this case, $i_1 = 20$, $i_2 = 10$, and k varied from 0.25 (i.e, Y/X = 0.25) to 10 (Y/X = 10). In this case, relatively complete parabolas were defined in each case, although again it should be remembered that the symbols denoting the end of each parabola represent the point at which the channels are open essentially 100% of the time. The apparent average single channel current from each σ^2/I relationship is shown in Fig. A1 (D). As the probability of being in i_2 is increased, the slope of the σ^2/I relationship not unexpectedly begins to approach the value of i_2. For this case when $i_2 = 0.5 i_1$, the weighted mean of the single channel currents is fairly similar to that estimated from the slope for the σ^2/I relationship.

Since Slo3 opens into conductance levels of ~55 and 110 pS and occupies both conductances about equally, on balance then, these considerations indicate that the estimates of Slo3 unitary current from σ^2/I analysis would be expected to be ~10–15% greater than the estimates from the averaged single channel opening (filled and open red circles in Fig. A1, B and D). Our estimates of apparent P_o from σ^2/I considerations will also be somewhat low compared with the true probability that the channels will be exclusively in open states. When $k = 1$, this error is ~10% (filled red diamonds in Fig. A1, B and D).

We thank Hai Jiang, Yimei Yui, and Yefei Cai for preparation of oocytes. We thank Rich Benzinger for assistance on derivations in Appendix.

This work was supported by National Institutes of Health grant GM066215.

Lawrence G. Palmer served as editor.

Submitted: 5 April 2006
Accepted: 8 August 2006

REFERENCES

Adelman, J.P., K.Z. Shen, M.P. Kavanaugh, R.A. Warren, Y.N. Wu, A. Lagrutta, C.T. Bond, and R.A. North. 1992. Calcium-activated potassium channels expressed from cloned complementary DNAs. *Neuron.* 9:209–216.

Bhattacharjee, A., L. Gan, and L.K. Kaczmarek. 2002. Localization of the Slack potassium channel in the rat central nervous system. *J. Comp. Neurol.* 454:241–254.

Bhattacharjee, A., W.J. Joiner, M. Wu, Y. Yang, F.J. Sigworth, and L.K. Kaczmarek. 2003. Slick (Slo2.1), a rapidly-gating sodium-activated potassium channel inhibited by ATP. *J. Neurosci.* 23:11681–11691.

Butler, A., S. Tsunoda, D.P. McCobb, A. Wei, and L. Salkoff. 1993. mSlo, a complex mouse gene encoding "maxi" calcium-activated potassium channels. *Science*. 261:221–224.

Cox, D.H., J. Cui, and R.W. Aldrich. 1997. Allosteric gating of a large conductance Ca-activated K^+ channel. *J. Gen. Physiol.* 110:257–281.

Hamill, O.P., A. Marty, E. Neher, B. Sakmann, and F.J. Sigworth. 1981. Improved patch-clamp techniques for high-resolution current recording from cells and cell-free membrane patches. *Pflugers Arch.* 391:85–100.

Hille, B. (2001) Ionic Channels of Excitable Membranes. 3rd ed. Sunderland Massachusetts, Sinauer Associates Inc.

Horrigan, F., and R. Aldrich. 2002. Coupling between voltage sensor activation, Ca^{2+} binding and channel opening in large conductance (BK) potassium channels. *J. Gen. Physiol.* 120:267–305.

Jiang, Y., A. Lee, J. Chen, M. Cadene, B.T. Chait, and R. MacKinnon. 2002. Crystal structure and mechanism of a calcium-gated potassium channel. *Nature*. 417:515–522.

Lingle, C.J. 2006. Empirical considerations in the use of ensemble-variance analysis of macroscopic currents. *J. Neurosci. Methods*. 10.1016/j.jneumeth.2006.05.027.

Schreiber, M., and L. Salkoff. 1997. A novel calcium-sensing domain in the BK channel. *Biophys. J.* 73:1355–1363.

Schreiber, M., A. Wei, A. Yuan, J. Gaut, M. Saito, and L. Salkoff. 1998. Slo3, a novel pH-sensitive K^+ channel from mammalian spermatocytes. *J. Biol. Chem.* 273:3509–3516.

Shi, J., G. Krishnamoorthy, Y. Yang, L. Hu, N. Chaturvedi, D. Harilal, J. Qin, and J. Cui. 2002. Mechanism of magnesium activation of calcium-activated potassium channels. *Nature*. 418:876–880.

Sigworth, F.J. 1980. The variance of sodium current fluctuations at the node of Ranvier. *J. Physiol.* 307:97–129.

Steffan, R., and S.H. Heinemann. 1997. Error estimates for results of nonstationary noise analysis derived with linear least squares methods. *J. Neurosci. Methods*. 78:51–63.

Wei, A., C. Solaro, C. Lingle, and L. Salkoff. 1994. Calcium sensitivity of BK-type KCa channels determined by a separable domain. *Neuron*. 13:671–681.

Xia, X.-M., X.-H. Zeng, and C.J. Lingle. 2002. Multiple regulatory sites in large-conductance calcium-activated potassium channels. *Nature*. 418:880–884.

Xia, X.-M., X. Zhang, and C.J. Lingle. 2004. Ligand-dependent activation of Slo family channels is defined by interchangeable cytosolic domains. *J. Neurosci.* 24:5585–5591.

Yuan, A., C.M. Santi, A. Wei, Z.W. Wang, K. Pollak, M. Nonet, L. Kaczmarek, C.M. Crowder, and L. Salkoff. 2003. The sodium-activated potassium channel is encoded by a member of the Slo gene family. *Neuron*. 37:765–773.

Zhang, X., X.-H. Zeng, and C.J. Lingle. 2006. Slo3 K^+ channels: voltage and pH dependence of macroscopic currents. *J. Gen. Physiol.* 128:317–336.